Contents lists available at ScienceDirect

Deep-Sea Research Part I

Spatial patterns of arctic sponge ground fauna and demersal fish are detectable in autonomous underwater vehicle (AUV) imagery

H.K. Meyer [a,*], E.M. Roberts [a,b], H.T. Rapp [a,c], A.J. Davies [b,d]

[a] Department of Biological Sciences and K.G. Jebsen Centre for Deep-sea Research, University of Bergen, P.O. Box 7803, N-5020, Bergen, Norway
[b] School of Ocean Sciences, Bangor University, Menai Bridge, Anglesey, LL59 5AB, UK
[c] NORCE, Norwegian Research Centre, NORCE Environment, Nygårdsgaten 112, 5008, Bergen, Norway
[d] Department of Biological Sciences, University of Rhode Island, Kingston, RI, 02881, USA

ABSTRACT

Deep-sea sponge grounds are important habitats that provide several ecosystem services, yet relatively little is known about their distribution and ecology. While most surveys have focused on the broad-scale distribution patterns of sponge grounds (100s–1000s m), only rarely have the finer-scale (<10 m) spatial distribution patterns of the primary organisms been studied. In this study, the autonomous underwater vehicle (AUV) *Hugin 1000* was used to map an area of an arctic sponge ground located on the summit of the Schulz Bank (Arctic Mid-Ocean Ridge), with the aim of detecting small-scale spatial patterns produced by the dominant megafauna. Using low-light cameras to construct a photomosaic comprising of 9,953 images and a virtual quadrat spatial sampling approach, density hotspots of the most prominent megafauna were visualized. The primary megafauna detected were demosponges, hexactinellids, ascidians, cnidarians, echinoderms, and demersal fish species. Most mega-fauna, like the primary structure-forming sponge species *Geodia parva* and *Stelletta rhaphidiophora*, were distributed evenly throughout the sample area, though species like *Lissodendoryx (Lissodendoryx) complicata* and *Gersemia rubiformis* displayed clear fine-scale spatial preferences. The three demersal fish species, *Macrourus berglax*, *Reinhardtius hippoglossoides*, and *Amblyraja hyperborea*, were uniformly distributed throughout the sample area. Based on the presence of skate egg cases and juveniles within many images, it is likely that the site is being used as a nursery ground for *A. hyperborea*. This study demonstrates the potential of using AUVs to detect fine-scale spatial patterns of the structure-forming sponges and demersal fish species. The use of AUVs for deep-water benthic surveys can help visualize how fauna (e.g. fish) utilise deep-sea habitats, and act as a tool for quantifying individuals through relatively unbiased means (e.g. pre-programmed track, no sampling). Such information is crucial for future conservation and management efforts.

1. Introduction

In the North Atlantic, between the 40° and 75° N latitude belt and depths of 150–1700 m, dense aggregations of large structure-forming sponges primarily of the *Geodia* genera can create habitats known as osturs or sponge grounds (Klitgaard and Tendal, 2004; Maldonado et al., 2016). Sponge grounds tend to form in a continuous or semi-continuous manner due to the patchy spatial distribution patterns of the primary sponge species (Beazley et al., 2013). This has made classifying sponge grounds through quantitative means difficult and led to inconsistencies in their definitions based on sampling techniques. For example, Klitgaard et al. (1997) defined sponge grounds as areas where the sponges make up 90% of the wet weight in non-fish trawl catches. However, in photographic surveys, sponge grounds are generally defined as areas with one sponge occurring every 1–30 m^2 (ICES, 2009), whereas in video-based surveys, they are classified as areas that contain 0.5–1 sponge per m^2 to 1 sponge per 10–30 m^2 (Hogg et al., 2010; Kutti et al., 2013). Regardless of the classification discrepancies, deep-sea sponge grounds have sparked scientific interest in recent years due to the recognition that they can support hotspots of biodiversity where they form structural habitat (Klitgaard and Tendal, 2004; Kutti et al., 2013; Maldonado et al., 2016).

Sponge grounds enhance habitat heterogeneity and biodiversity by providing a number of ecological services (Buhl-Mortensen et al., 2010;

---

* Corresponding author.
  E-mail address: Heidi.Meyer@uib.no (H.K. Meyer).

Beazley et al., 2013, 2015; Hawkes et al., 2019). Similar to cold-water coral reefs (e.g. Costello et al., 2005), many fish and invertebrate species appear to exploit sponge grounds as spawning, nursery and foraging grounds, areas of refuge, and additional substrate (Kenchington et al., 2013; Kutti et al., 2013; Hawkes et al., 2019). When actively filtering, sponges recycle carbon, nutrients, and dissolved organic matter back into the environment (de Goeij and van Duyl, 2007; de Goeij et al., 2013; Howell et al., 2016; McIntyre et al., 2016). Through this cycling process, sponge grounds transfer excess energy to upper trophic levels and improve bentho-pelagic coupling (Bell, 2008; Cathalot et al., 2015). The canals, cavities, and porous exterior of sponges generate various microhabitats that are utilised by small organisms for protection against strong currents or predation (Klitgaard and Tendal, 2004; Buhl-Mortensen et al., 2010), and the spicule mats formed from deceased sponges create additional substrate for epibenthic fauna (Bett and Rice, 1992; Beazley et al., 2015; McIntyre et al., 2016). Increasingly, sponge grounds are thought to be highly important to other local fauna similar to cold-water coral reefs (Beazley et al., 2013, 2018; Cathalot et al., 2015; Hawkes et al., 2019). However, there is limited information about the ecology and distribution of deep-sea sponges, particularly at small scales (<10's m).

The majority of studies on deep-sea sponge grounds have investigated the community composition, distribution patterns, and abiotic drivers over broad scales (100's – 1000's m), ranging from topographic features, such as the Flemish Cap (Murillo et al., 2012; Beazley et al., 2013) and Sackville Spur (Beazley et al., 2015), to oceanic regions, such as the Canadian Arctic (Murillo et al., 2018), Northeast Atlantic (Klitgaard and Tendal, 2004), Northwest Atlantic (Knudby et al., 2013), and North Atlantic (Howell et al., 2016). The broad-scale distribution of deep-sea sponge grounds is found to be influenced by a variety of abiotic drivers, such as increased dissolved silicate levels (Howell et al., 2016), low temperatures (Klitgaard and Tendal, 2004; Howell et al., 2016), minimum bottom salinity (Knudby et al., 2013; Beazley et al., 2015), bottom current speed (Beazley et al., 2015), particulate organic carbon flux (Howell et al., 2016), and depth (Knudby et al., 2013; Beazley et al., 2015; Howell et al., 2016). While depth is consistently identified as a top driver for sponge ground distribution over broad-scales (Beazley et al., 2015; Howell et al., 2016), it acts as a proxy for other variables (e.g. temperature, salinity, and water mass). Over such broad scales, environmental conditions and habitat structure will change, and while previous findings provide significant insight into the abiotic variables that vary over large spatial scales, there is very little known about the variables that are important at local scales. As such, there is a clear knowledge gap regarding the drivers of the small-scale patterns observed in the main inhabitants of individual sponge grounds. Understanding these patterns and their respective drivers provides insight into ecological interactions operating within deep-sea ecosystems (Robert et al., 2014).

Given the expected vulnerability of these deep-sea habitats to disturbance and climate change (OSPAR, 2008; FAO, 2009; Hogg et al., 2010), there is an urgent need to identify and map the distribution of primary structure-forming sponge species, and to assess the factors influencing sponge ground formation, persistence, and community composition (Hogg et al., 2010; Kutti et al., 2013; Beazley et al., 2015, 2018; Howell et al., 2016; Roberts et al., 2018). To date, a variety of surveying techniques have been used for these purposes. Traditional extractive methods such as scientific trawling and dredging have been used extensively for large-scale benthic surveys (Klitgaard and Tendal, 2004; Knudby et al., 2013; Morris et al., 2014; McIntyre et al., 2016); however, such methods do not capture the patterns that occur at the fine-scales (i.e. within sponge grounds). Non-extractive methods like visual-based surveys conducted by towed-camera systems or submersibles have become a favoured tool as they allow for continual observations of the benthos and are relatively non-intrusive (Sánchez, 2009; Marsh et al., 2013). Photographic surveys can provide abundance estimates for the larger benthic megafauna and are thought to be more

realistic than those from extractive methods (Williams et al., 2015). This can help identify areas of specific biological interest (e.g. deep-sea fish species, vulnerable marine ecosystems), community structure, and zonation patterns through finer-scale analysis of georeferenced imagery (Ludvigsen et al., 2007; Marsh et al., 2013). One tool that is gaining in popularity is the creation of photomosaics from imagery data, which make it possible to visualise localised habitat composition and its seafloor extent through quantitative spatial analysis (Sánchez et al., 2009; Robert et al., 2017).

Submersibles like remotely operated vehicles (ROVs) or autonomous underwater vehicles (AUVs) have greatly improved what is currently known about the deep sea (Danovaro et al., 2014). In addition to visualising the seafloor using cameras or acoustic sensors, environmental parameters like temperature, salinity, dissolved oxygen, and depth can be measured simultaneously during the survey (Wynn et al., 2014). ROVs have some benefits over AUVs, for example, they are capable of collecting specimens for taxonomic validation of the video data and surveys can be easily altered by operators when discovering features of interest (Thresher et al., 2014; Howell et al., 2014; Williams et al., 2015). However, they can be influenced by swell and have relatively slow transect speeds (Morris et al., 2014), which can affect altitude, direction, and speed along transects. AUVs, on the other hand, autonomously traverse a specified route within fixed altitude limits (Wynn et al., 2014), minimising human interaction and operator error, giving them an advantage as a survey-tool over ROVs. As such, image-based surveys conducted using AUVs are emerging as an important tool for the exploration of deep-sea habitats and quantitative mapping of benthic megafauna (e.g. Statham et al., 2005; Grasmueck et al., 2006; Kelly et al., 2014; Huvenne et al., 2016).

Previous studies have shown photographic surveys to be a promising means of investigating deep-sea communities such as cold-water coral reefs, hydrothermal vent fields, and sponge grounds (Beazley et al., 2013; Morris et al., 2014; McIntyre et al., 2015; Bell et al., 2016; Milligan et al., 2016; Robert et al., 2017). However, few studies have solely used visual-based surveys for mapping sponge grounds in detail (e.g. Kutti et al., 2013; Hawkes et al., 2019), even fewer with an AUV (e.g. Powell et al., 2018). Additionally, no known study has used AUV imagery to investigate the small-scale spatial patterns produced by individual species within a sponge ground.

In this study, AUV imagery was used to map the spatial patterns of megafauna and demersal fish in an arctic sponge ground on the summit of the Schulz Bank, located on the Arctic Mid-Ocean Ridge. The aims of the study are as follows: (1) detect megafauna (≥1 cm) inhabiting the Schulz Bank sponge ground through AUV imagery; (2) map the fine-scale spatial patterns produced by the most prominent megafauna (≥0.5% of the total abundance); (3) study the influence of the measured abiotic variables on the community patterns and most prominent megafauna; (4) characterise the demersal fish population; and (5) investigate whether this is a potential nursery ground for demersal fish.

2. Materials and methods

2.1. Study area

The Schulz Bank (73° 47′ N, 7° 40′ E), previously reported as the Schultz Massif or Massive (Cárdenas et al., 2011, 2013; Roberts et al., 2018), is a deep-sea seamount located at the Arctic Mid-Ocean Ridge (AMOR) where Mohn's Ridge transitions into the Knipovich Ridge. It rises from water depths greater than 2500 to 560 m at the summit (Fig. 1). The surrounding area has been extensively surveyed in recent years owing to nearby hydrothermal activity, specifically the Loki's Castle vent field (Pedersen et al., 2010; Olsen et al., 2015; Steen et al., 2016). The sponge composition on the Schulz Bank and nearby sponge ground regions are largely dominated by demosponges such as *Geodia parva, G. phlegraei, G. hentscheli, Stelletta rhaphidiophora, Craniella infrequens, Thenea valdivae, Hexadella dedritifera, Polymastia thielei* (Cárdenas
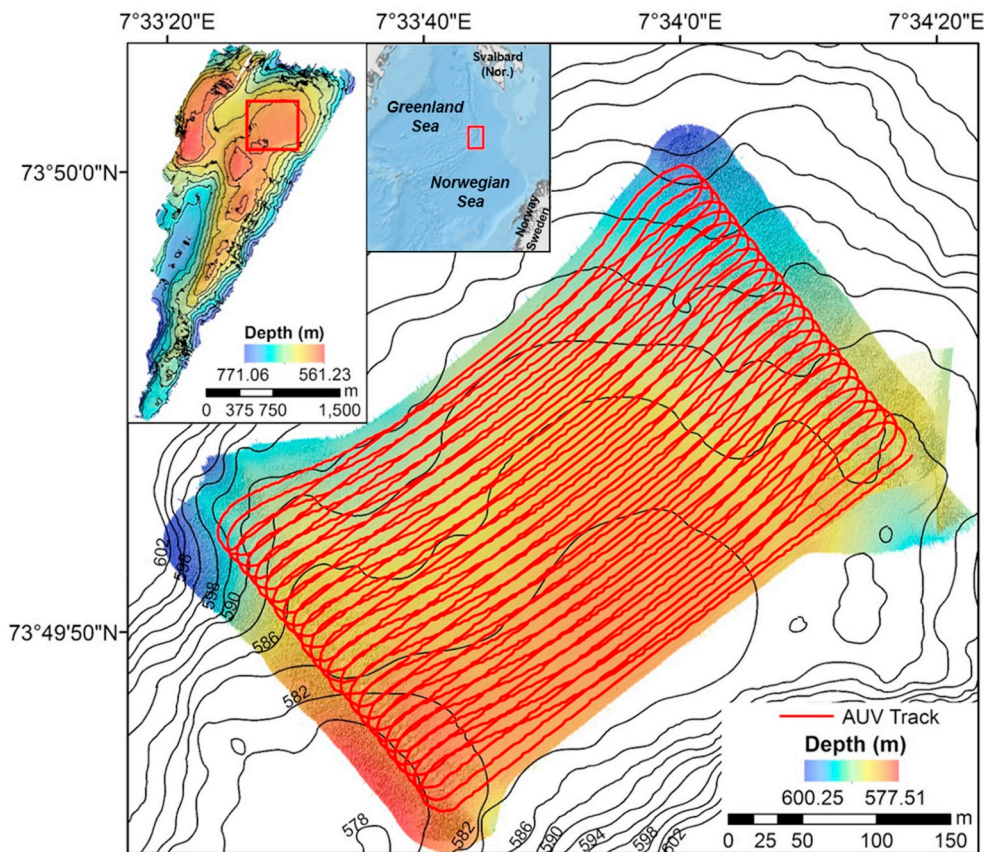
Fig. 1. Multibeam bathymetry of the Schulz Bank summit and the selected sample area. The red box on entire seamount (first inset) indicates the sample area, the second inset shows the location of Schulz Bank on the Arctic Mid-Ocean Ridge. Red lines in the main figure show the *Hugin 1000* track within the sampling area. Bathymetric contours in the sampling area are every 2 m. The black contour lines on the entire seamount (first inset) represent every 20 m. (For interpretation of the references to colour in this figure legend, the reader is referred to the Web version of this article.)

et al., 2011, 2013; Plotkin et al., 2018; Roberts et al., 2018), intermixed with a variety of hexactinellid species such as *Schaudinnia rosea, Scyphidium septentrionale, Trichasterina borealis,* and *Asconema foliata* (Klitgaard and Tendal, 2004; Maldonado et al., 2016; Roberts et al., 2018).

The physical oceanography of the Nordic Seas region is described in Hopkins (1991), Mauritzen (1996) and Hansen and Østerhus (2000). The Schulz Bank is a prominent feature of the AMOR system and is subject to a complex oceanographic setting, as is further described in Roberts et al. (2018). Three main water masses tend to dominate at the Schulz Bank: (1) the surface water mass above the seamount consists of the relatively warm and high salinity Norwegian Atlantic Water; (2) the base and flanks of the seamount are exposed to the colder, fresher Upper Norwegian Deep Water; and (3) an intermediate water mass impinges upon the seamount summit and shallower areas and is likely to be Norwegian Arctic Intermediate Water (Jeansson et al., 2017; Roberts et al., 2018). It may be influenced by topographically-steered deep currents (Orvik and Niiler, 2002), and tidally-driven internal motions are thought to be important to filter feeders inhabiting the summit (Roberts et al., 2018).

For the present study, a gently sloping section of the summit was selected as the primary focus for an in-depth AUV survey (Fig. 1). This had an area of approximately 0.12 km^2 (water depth range: 577–600 m). Soft sediment and a dense spicule mat were characteristic of the substrate on the summit, with little to no visible hard substrate, beyond the occasional boulder.

2.2. Data collection

The seamount was investigated in June 2016 using the RV *G.O. Sars*. Imagery and bathymetric data for the sample area on the summit were collected using AUV *Hugin 1000*. The AUV flew at an average altitude of 5.0 m, with a respective minimum and maximum altitude of 3.8 and 8.5 m, excluding vehicle turns, along a 47 track-line path above the seafloor (Fig. 1). The AUV was fitted with a SAIV SD208 dual conductivity, temperature, and depth (CTD) system, Kongsberg HISAS 1030 synthetic aperture sonar, a Kongsberg EM2040 multibeam echosounder, and a downwards-looking TileCam optical camera. The camera was located approximately 1 m behind the LED light bar (720 LEDs) to reduce the impact of backscattered light. It had a 10-megapixel resolution and a 10-gigabyte hr^{-1} collection rate.

2.3. Environmental data

All spatial data were converted to Universal Transverse Mercator projection (Zone 31° N) to allow for area calculations. EM2040 data was processed with the Reflection AUV post-mission analysis software (version 3.1.0) by Kongsberg Maritime, and the projected bathymetric data of the seamount and sampling area extracted. The final bathymetric grid created had a cell size of 0.1 × 0.1 m. Slope (°), aspect (°), and topographic roughness were calculated from bathymetry using the Digital Elevation Model Surface Tools (Jenness, 2013) within ArcGIS 10.4 (ESRI). *In situ* temperature (°C) and salinity (psu) data obtained from the AUV's CTD system were interpolated using inverse distance weighting (IDW) to create a continuous representation of the conditions on the summit at a resolution of approximately 0.6 × 0.6 m for both variables.

2.4. Image processing

A photomosaic was constructed automatically using Reflection to visualize the sample area and the location of the images to examine the spatial relationships of the fauna, species composition, and community structure of the sponge ground. Images were automatically converted to grey scale by Reflection before stitching successive images together into

a track-line mosaic (Fig. 2). Image area was calculated from Reflection using the AUV position data.

Images were selected for analysis based on the following criteria: (1) AUV altitude was between 4.7 and 5.3 m to maintain image quality (e.g. good scene illumination, consistent altitude, taxonomic resolution, exclude vehicle turns); (2) images were separated by at least 5 m to reduce the risk of using overlapping images that capture the same feature twice (Bell et al., 2016); and (3) images did not display signs of corruption or digital artefacts which could mar interpretation. Image corruption occurred when the Tilecam optical camera wrote over an image with a successive image before the file was completed and stored, thus resulting in an overlap of images on a single file. There were 9,953 images collected by the AUV over 2.78 h, at approximately 1 s intervals. Only 5,611 images (56.4%) fit the criteria and a subset of 430 images were selected for analysis. Images that fit the criteria are hereafter referred to as "optimal images" and the subset of images that were selected for analysis are hereafter referred to as "selected images".

To make sure the selected images were separated by at least 5 m from other selected images, a pseudorandom selection process was conducted whereby selected images separated by 5–20 optimal images were randomly selected along each track-line. The selected images were then checked to ensure they did not contain overlapping features or corruption. Colour versions of the selected images were used to confirm species identification and corruption status. Due to inconsistent illumination, each selected image was overlain with a 2.5×2.0 m digital quadrat, which was placed in the top centre portion of the image to exclude image areas that had poor visibility and allow for quantitative spatial sampling (Fig. 2). Each selected image had an average area of $16.23 \, m^2$ $(SD = 0.74 \, m^2)$ and was separated from its nearest neighbouring selected images by a mean distance of 9.6 m (SD = 2.44 m). The minimum and maximum distance of separation was 5.56 and 24.83 m, respectively. The mean altitude for both the selected images and optimal images was 4.93 m with a standard deviation (SD) of 0.11, indicating the AUV operated at stable altitude (Morris et al., 2014).

2.5. Identification of fauna

Only epibenthic megafauna and demersal fish visible within the quadrat were enumerated and identified to the lowest taxonomic level possible. Any indication that the sponge ground was being used as a nursery for the demersal fish, such as such as egg cases or juvenile demersal fish, were documented. As is common with imagery analysis, not all fauna were identified to species level due to the relatively low morphological detail visible (Sánchez et al., 2009; Bell et al., 2016). The identifications of the megafauna and demersal fish were quality checked and agreed upon by the authors, and identifications confirmed by physical samples collected from the summit. As a result of the quality check and difficulties in consistent identification of certain species within the selected images, the suspected species *Thenea valdiviae* and *Craniella infrequens* were grouped as 'Demospongiae spp.' and *Schaudinnia rosea, Trichasterina borealis,* and *Scyphidium septentrionale* were grouped as 'Hexactinellida spp.' after the annotation process.

2.6. Demersal fish population

After the initial annotation revealed that the demersal fish and *Amblyraja hyperborea* egg cases were often present outside of the quadrat or in nearby optimal images, a secondary annotation was conducted on all optimal images to assess the demersal fish population and investigate the area as a nursery ground for *A. hyperborea*. All further mentions of the initial annotation and secondary annotation will hereby be referred to as "megafauna survey" and "fish survey", respectively.

All fish and egg cases within the whole optimal image were counted because they were easily identifiable within the images and had a high likelihood of remaining visible even when present outside of the quadrat. In addition, fish were documented as swimming (i.e. appeared in motion, above the substrate, or visible shadow) or non-swimming (i.e. placed directly on the substrate, lack of shadow) in the optimal images. It was also noted if there appeared to be a change in fish behaviour between optimal images that contained the same fish (e.g. non-swimming to swimming between images) (Stoner et al., 2008). To avoid double-counting of the same individual, successive and nearby images within the sample area were checked to ensure the images did not overlap or the individual did not move. Images that contained the same fish individual(s) were dropped from analysis. As it was too difficult to differentiate between decaying and fresh skate eggs, all visible egg cases were counted within an image.
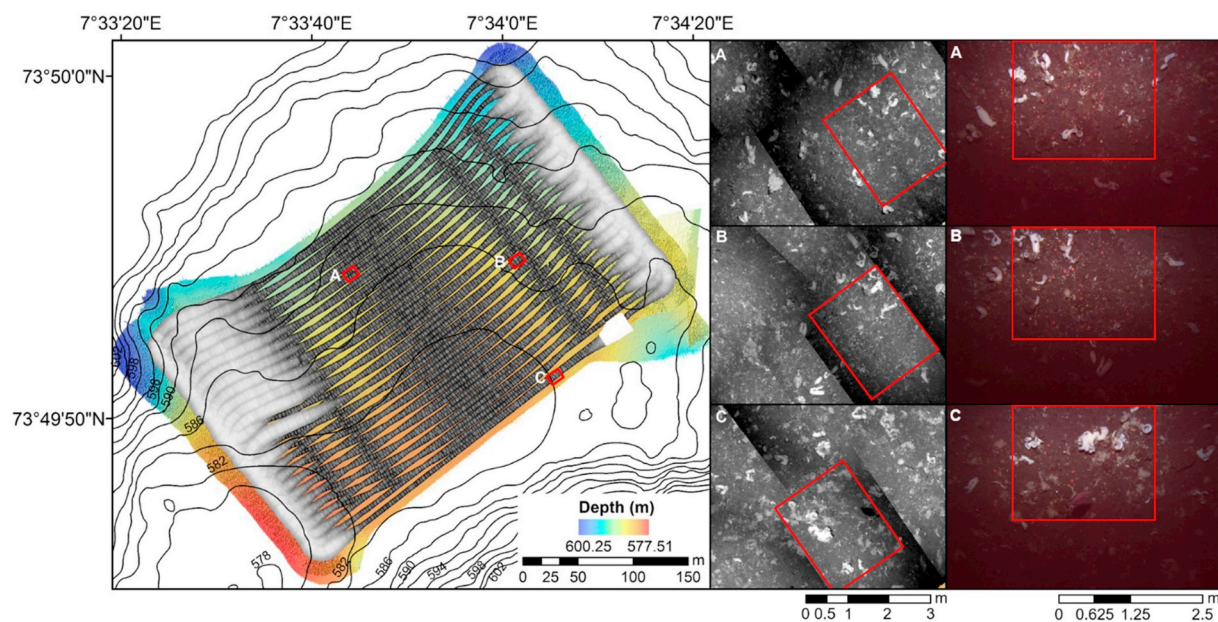

Fig. 2. Photomosaic of the sample area on Schulz Bank with examples of the image mosaic. The labelled red squares on the map indicate the location of example images from the mosaic (second column). The third column show the individual colour image from each area, emphasising the $5 \, m^2$ quadrat used for analysis. (For interpretation of the references to colour in this figure legend, the reader is referred to the Web version of this article.)

2.7. Statistical analysis

2.7.1. Preparation of megafauna data

All taxa with confirmed identities from the quality check were included in the analysis, and taxa that made up ≥0.5% of the total abundance were classified as the "most prominent megafauna". To allow for easier comparison between different surveys, the raw taxon abundance observed in each selected image was converted to density (ind. m^{-2}) (Kutti et al., 2013). All statistical analysis was conducted in RStudio (version 1.1.383; RStudio Team, 2016) unless otherwise specified.

2.7.2. Environmental influence

To determine which, if any, abiotic variables and prominent megafauna densities were correlated, a Spearman's rank correlation coefficient matrix was generated with the package "Hmisc" (version 4.1–1; Harrell Jr., 2018). The *in situ* abiotic conditions demonstrated little variation within the sample area. Depth in the selected images had a range of 579.4–590.8 m and was found to be significantly correlated with temperature, salinity, and topographic roughness, in addition to the majority of the prominent megafauna densities (S1). However, it was selected to remain in the analysis because depth often acts as a proxy for other abiotic variables that were not measured or described in the present study. There were only small differences in temperature and salinity between sampled image locations (0.005–0.078 °C and 35.00–35.04 psu, respectively). Topographic roughness, slope, and aspect also demonstrated little variation, and the overall bottom structure was fairly homogeneous.

Regardless of the apparent homogeneity in abiotic conditions, negative binomial generalized additive models (GAMs) were constructed using R package "mgcv" (version 1.8–24; Wood, 2011) to identify which environmental variables best explained the variance in the community data (e.g. species richness and total megafauna abundance) and the most prominent megafauna abundance data (Zuur et al., 2009). GAMs were selected over a generalized linear models (GLMs) because either not all explanatory variables displayed a linear trend with the community data or most prominent megafauna abundance data, or there was no clear relationship between the response variables and the entire explanatory variables (Zuur et al., 2009). The environmental variables that were included in the GAM analysis were depth (m), temperature (°C), salinity (psu), aspect (°), slope (°), and topographic roughness. Quadrat size was offset to account for the abundance within each quadrat and to obtain estimates that reflected density. Thin plate regression splines were used as smoothing functions applied to each of the abiotic variables (Zuur et al., 2009). To reduce the chance of over-fitting of the smooth-functions of the model, a gamma function was used (Zuur et al., 2009).

2.7.3. Sponge ground community and demersal fish patterns

Kernel density estimates (KDEs) were calculated for the most prominent megafauna, demersal fish, and skate egg cases in ArcGIS to visualise their spatial patterns on the summit and identify areas of dense aggregation within the sample area (Kenchington et al., 2014; Beazley et al., 2018). KDE calculations were conducted using a neighbour-based approach that fits a smoothing curve over the data points using the quartic kernel function as described by Silverman (1986). The values of the kernel surfaces overlaying raster cell centres were summed together to generate density estimates for each output raster cell. The smoothing curve is highest at the central point and gradually decreases with the search radius. Therefore, the more data points that fall within the search radius, the more smoothed the output raster becomes. The search radius selected was 20 m to include neighbouring data points for optimal smoothing based on the average neighbour distance between selected images (see section 3.1). The output cell size was 0.6 × 0.6 m and selected based on the resolution of the base map.

Based on the kernel density plots and visible spatial patterns along the depth gradient, regression analysis was conducted on the nine most prominent megafauna to examine the relationship between the density (ind. m^{-2}) and depth (m) using the "car" (version 3.0–2; Fox and Weisberg, 2011) package in R. Regression analyses were also conducted on the demersal fish and skate egg abundances (ind. image^{-1}). Taxa that displayed a non-linear trend were analysed with the non-linear least squares function. To check if the relative patterns were preserved after smoothing from the KDE calculations and that over-smoothing had not occurred, regression plots for the prominent megafauna KDEs against depth (m) were compared to the respective density regression plots (S2).

3. Results

3.1. Prominent megafauna

There were 20 morphotypes detected within the selected images (Table 1 and Fig. 3), and were in the following classes: Ascidiacea (1), Hexactinellida (1), Demospongiae (8), Anthozoa (2), Asteroidea (3), Echinoidea (1), Actinopterygii (2), Chondrichtyes (1), and Malacostraca (1). The most prominent megafauna that contributed to ≥0.5% of the total abundance present in the images were ascidians, anemones, demosponges (Demospongiae spp., *Lissodendoryx (Lissodendoryx) complicata*, *Hexadella dedritifera*, *Geodia parva*, *Stelletta raphidiophora*), Hexactinellida spp., and *Gersemia rubiformis*. Mobile fauna such as echinoderms and demersal fish had a low occurrence during the megafauna survey because they were rarely observed within the confines of the quadrat.

3.2. Environmental influence

The GAM analysis showed the measured environmental variables explained relatively little of the variation in species richness (GAM: total deviance explained = 6.74%; S3) or total megafauna abundance (GAM: total deviance explained = 33.14%; S4). Depth most influenced the variability within community patterns (Table 2). Similar trends were observed for the most prominent megafauna data (S5 to S14).
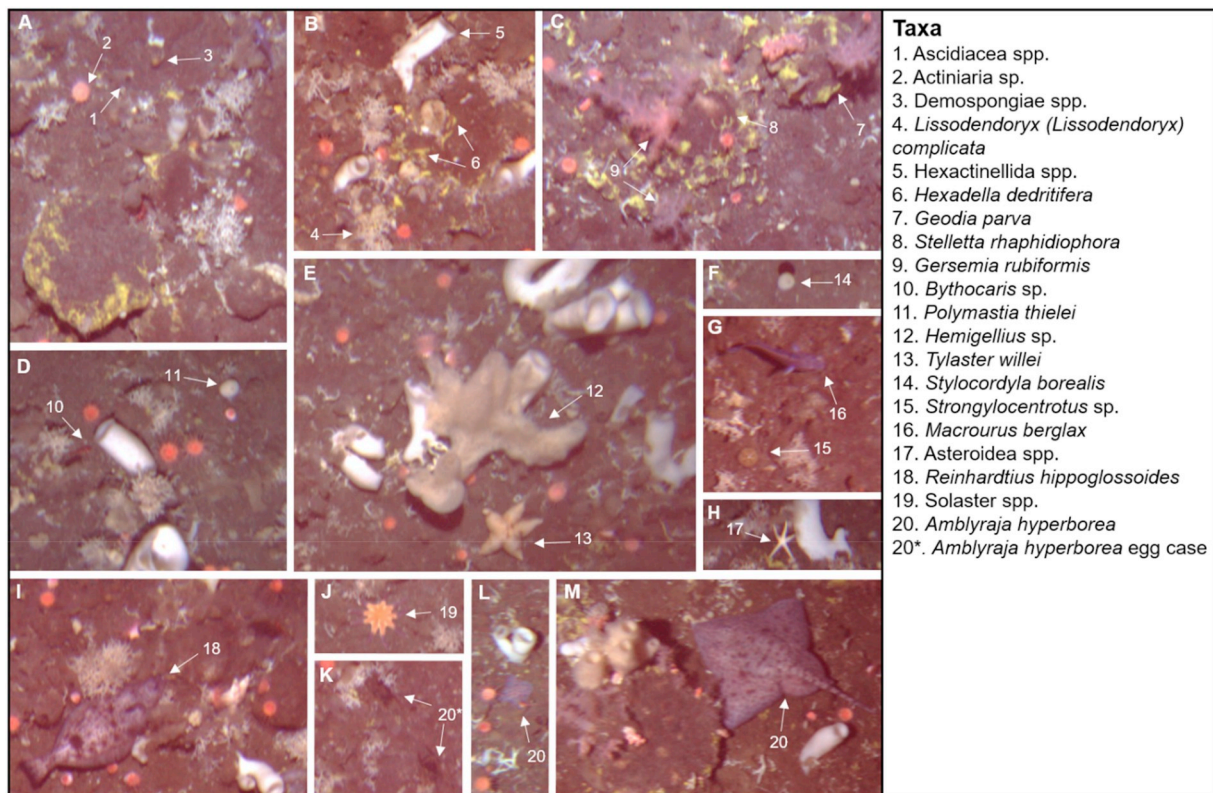
3.3. Sponge ground community patterns

Ascidians were the most abundant taxa within the sample area and present within every image. Their densities were often double that of the

Table 1
Abundance of the prominent megafauna found on the Schulz Bank summit in the megafauna survey.

Phylum	Taxa	Total Abundance
Arthropoda	*Bythocaris* sp. G.O. Sars, 1870	348
Chordata	Ascidiacea spp.	35,952
	Amblyraja hyperborea (Collet, 1879)	4
	Macrourus berglax Lacépède, 1801	42
	Reinhardtius hippoglossoides (Walbaum, 1792)	17
Cnidaria	Actiniaria sp.	19,074
	Gersemia rubiformis (Ehrenberg, 1834)	691
Echinodermata	*Tylaster willei* Danielssen and Koren, 1881	183
	Asteroidea spp.	29
	Solaster spp. Forbes, 1839	8
	Strongylocentrotus sp. Brandt, 1835	78
Porifera	Demospongiae spp.	15,050
	Geodia parva Hansen, 1885	1,713
	Hemigellius sp. Burton, 1932	204
	Hexadella dedritifera Topsent, 1913	5,197
	Hexactinellida spp.	5,489
	Lissodendoryx (Lissodendoryx) complicata (Hansen, 1885)	7,331
	Polymastia thielei Koltun, 1964	251
	Stelletta rhaphidiophora Hentschel, 1929	1,344
	Stylocordyla borealis (Lovén, 1868)	177

Fig. 3. Examples of megafauna observed on the Schulz Bank summit. Taxa categorized by the most abundant megafauna to the least abundant observed within the megafauna survey.

Table 2
Summary statistics of the generalized additive models fitted to the species richness (S) and total megafaunal abundance (N) (negative binomial distribution, log link). Deviance explained (%) is the percent of null deviance in the data explained by the model. All abiotic variables contained a smoothing function (see S3 and S4).

Response	Explanatory	Deviance Explained (%)	R^2	P-value
Species Richness	Depth (m)	5.05	0.0431	0.001
	Temperature (°C)	1.49	0.0128	0.011
	Salinity (psu)	0.08	−0.0015	0.560
	Slope (°)	0.04	−0.0019	0.670
	Aspect (°)	0.04	−0.0020	0.901
	Topographic Roughness	0.03	−0.0020	0.707
Total Megafauna Abundance	Depth (m)	26.60	0.2580	<0.001
	Temperature (°C)	4.34	0.0406	0.002
	Salinity (psu)	0.15	0.0008	0.419
	Slope (°)	1.62	0.0100	0.335
	Aspect (°)	0.01	−0.2240	0.836
	Topographic Roughness	0.43	0.0012	0.145

Table 3
Density (ind. m^{-2}) summary of the most prominent megafaunal species within the selected images the taxon was observed in.

Taxa	Number of Images	Minimum	Maximum	Average ± SE
Ascidiacea spp.	430	3.00	40.60	16.52 ± 0.30
Actiniaria sp.	430	2.20	22.20	8.87 ± 0.17
Demospongiae spp.	430	2.00	14.20	7.00 ± 0.11
Lissodendoryx (Lissodendoryx) complicata	419	0.20	11.60	3.50 ± 0.12
Hexactinellida spp.	430	0.40	6.20	2.55 ± 0.05
Hexadella dedritifera	429	0.20	6.20	2.42 ± 0.05
Geodia parva	411	0.20	2.40	0.83 ± 0.02
Stelletta rhaphidiophora	381	0.20	3.20	0.71 ± 0.02
Gersemia rubiformis	244	0.20	2.80	0.57 ± 0.03

next most prominent taxa, the anemones (Table 3). The ascidians were commonly growing directly on the spicule mat and along the edges of large demosponges. They were often used as substrate for other sessile megafauna, predominantly the anemones. Ascidians were more densely aggregated in the deeper north-western region of the sample area (Figs. 4 and 5) and demonstrated a positive correlation with increasing water depth ($R^2 = 0.239$, $p < 0.001$). Unsurprisingly given their co-occurrence with ascidians, the anemones were also significantly correlated with depth ($R^2 = 0.221$, $p < 0.001$), although their density hotspot displayed more signs of patchiness compared to the ascidians (Fig. 4).

Demospongiae spp. had a widespread distribution throughout the

sample area and had no significant change in density with depth (Figs. 4 and 5). *Lissodendoryx (Lissodendoryx) complicata* was most densely aggregated in the south-eastern portion of the sample area and its distribution strongly followed the 586 m depth contour (Fig. 4). Deeper than this, the species' density rapidly declined, and occurrences thinned considerably into small patches. Its density demonstrated a statistically significant negative exponential relationship with depth (Nonlinear Least Squares: $p < 0.001$; Fig. 5). Hexactinellida spp. did not exhibit any spatial preference on the summit and were distributed evenly throughout the sample area.

The yellow encrusting sponge, *H. dedritifera*, was primarily observed growing on the large demosponges, *G. parva* and *S. rhaphidiophora*. While *G. parva* and *S. rhaphidiophora* were observed in low densities in the present study (Table 3), their large size makes them likely to contribute considerably to the overall megafaunal biomass. The three demosponge species were present throughout the sample area with some signs of spatial patchiness, though only *H. dedritifera* displayed a slight
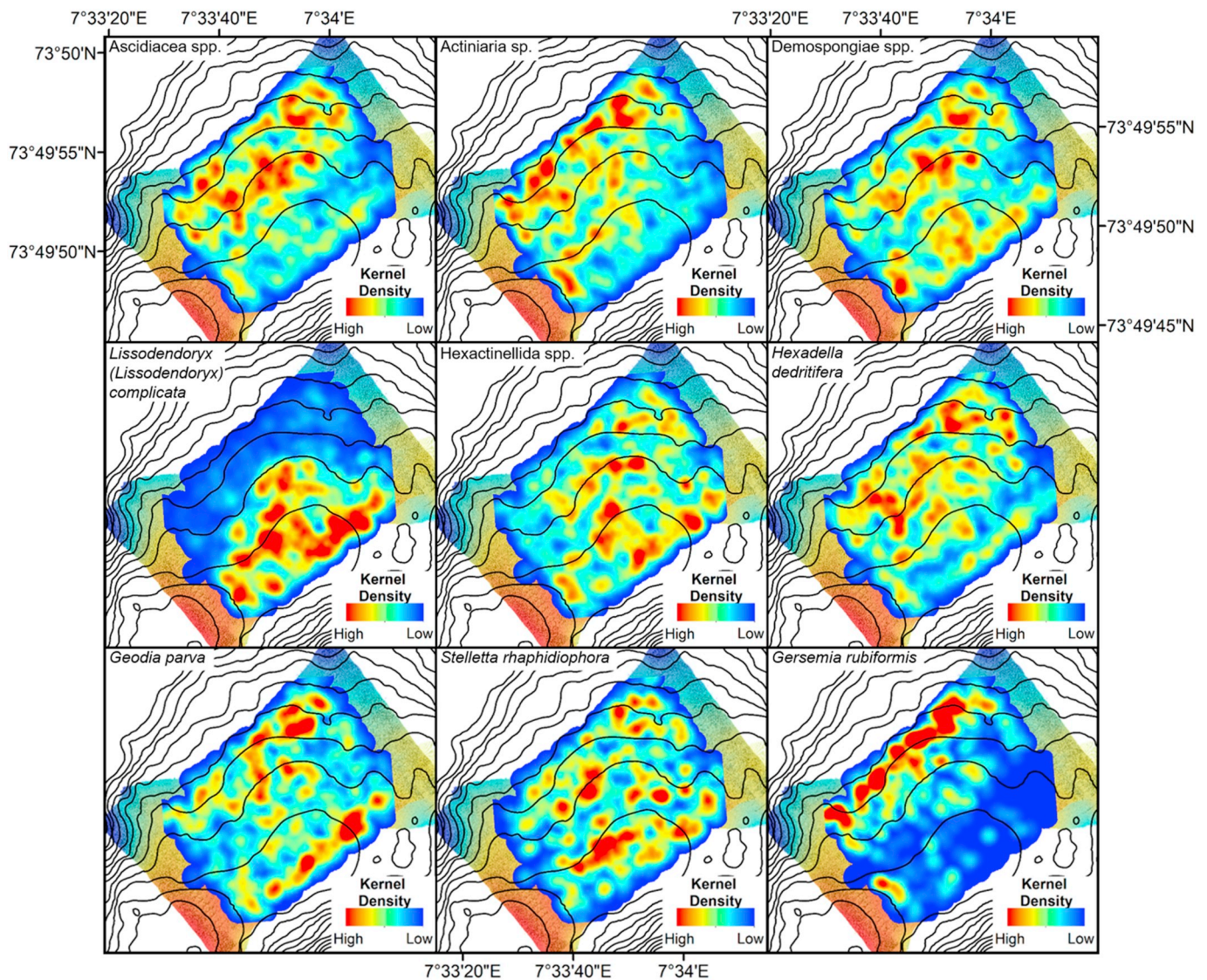
Fig. 4. Kernel density estimation plots of the most prominent megafauna on the Schulz Bank summit determined from the *Hugin 1000* imagery. Contour lines represent every 2 m and are as shown in Fig. 1. Kernel density values are normalized by the maximum densities occurring for each species.

significant positive trend with increasing water depth ($R^2 = 0.131$ $p < 0.001$).

The soft coral, *G. rubiformis* had a very patchy distribution and was only present in the north-western edges of the sample area. It became more abundant at depths greater than 586 m, and demonstrated a positive exponential relationship with depth (Nonlinear Least Squares: $p < 0.001$; Fig. 5).

3.4. Demersal fish on the summit

The summit was inhabited by three observable demersal fish species (n = 708 individuals) (Fig. 6), which were present within 662 images (11.8 % of optimal images). In any given image, there was a maximum of three individuals present.

The most common species was the Roughhead Grenadier (*Macrourus berglax*, Fig. 3G), which accounted for approximately 68.2% of the total observed fish abundance (n = 483 individuals). *Macrourus berglax* were always observed above the substrate and in motion. It was unclear whether there was a change in behaviour between images that contained the same individual.

The second most abundant species was a commonly targeted commercial species, the Greenland Halibut (*Reinhardtius hippoglossoides*,

Fig. 3I), which accounted for approximately 25.0% of the total fish population. *Reinhardtius hippoglossoides* were observed swimming (n = 110 individuals) more often than non-swimming (n = 67 individuals).

The Arctic Skate (*Amblyraja hyperborea*, Fig. 3M) was the least abundant fish observed and accounted for 6.8% of the population (n = 48 individuals), and 27% of the skates observed were juveniles (Fig. 3L). Overlapping images that contained the same *A. hyperborea* individuals were separated by approximately 5 min. The individuals were seemingly undisturbed by the AUV because they did not move between images. All fish species appeared to be randomly distributed on the summit and displayed little spatial preference, and no specific epifaunal taxa association or depth (linear regression: p > 0.01; S15).

Amblyraja hyperborea egg cases were regularly observed throughout the sample area, often directly on the spicule mat (Fig. 6). They were present in 49.3% of all optimal images with a total abundance of 4061 eggs (n = 2769 images). The highest abundance of eggs in a single image was 6 eggs (n = 3 images), though most images only contained 1 egg (n = 1840 images). There appeared to be higher accumulations of eggs in the south-eastern region, the shallower section, of the sample area. However, the skate eggs displayed a weak relationship with depth ($R^2 = 0.030$, $p < 0.001$; S15).
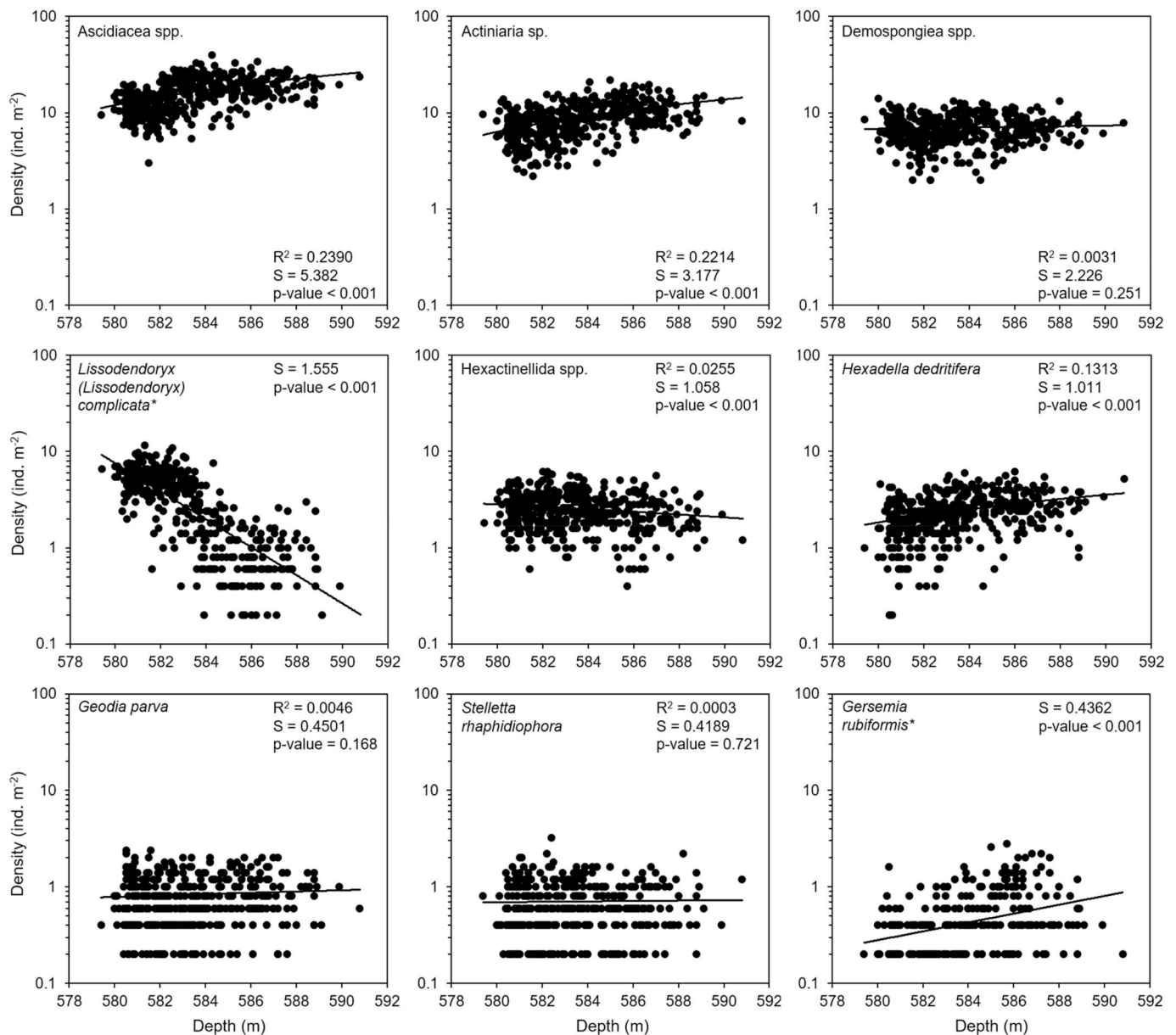
Fig. 5. Regression plots of density (ind. m^{-2}) against depth (m) for the most prominent megafauna on the Schulz Bank. Y-axes have been semi-logged to standardize the differences in densities between megafauna. Residual standard error (S) and R-squared show the statistical correlation of the relationship between density and depth. Asterisks (*) denotes taxa which had a non-linear relationship with depth.

4. Discussion

To the authors' knowledge, this study is the first that has utilised an AUV to map a deep-sea sponge ground in the North Atlantic and one of the very few studies to use an AUV to study the spatial distribution of deep-sea fish assemblages (Milligan et al., 2016; Powell et al., 2018). The AUV imagery provided insight of the major megafauna taxa inhabiting the sponge ground and detected the spatial patterns of the most prominent megafauna and demersal fish species. The presence of *Amblyraja hyperborea* egg cases and juveniles suggests the area may be used as a nursery ground.

4.1. Sponge ground on the summit

Geodia species are commonly the primary structure-forming sponge species found in sponge grounds in the North Atlantic (Klitgaard and Tendal, 2004; Cárdenas et al., 2013; Howell et al., 2016). Several species

that were observed in the present study have previously been classified as indicator species or habitat builders of arctic sponge grounds (Cárdenas et al., 2013; Maldonado et al., 2016; Murillo et al., 2018). For example, Murillo et al. (2018) suggested that *G. hentscheli*, *G. parva*, and *S. rhaphidiophora* are indicative of arctic sponge grounds, and *L. complicata* can be considered an indicator of arctic slope sponge habitats (Mayer and Piepenburg, 1996). Additionally, as observed on the Schulz Bank, the hexactinellid sponge species *T. borealis* and *S. rosea*, are common in arctic sponge grounds (Maldonado et al., 2016).

The densities of the primary structure-forming sponges fit within all of the sponge ground definitions that have been previously suggested, where there are at least one sponge occurring every 1–30 m^2 (ICES, 2009), the sample area does contain 0.5–1 sponge per m^2 to 1 sponge per 10–30 m^2 (Hogg et al., 2010; Kutti et al., 2013), and the sponges are occurring in a continuous or semi-continuous fashion (Beazley et al., 2013). Based on the stated variables and presence of common arctic sponge ground species (Murillo et al., 2018), it is clear that the sample
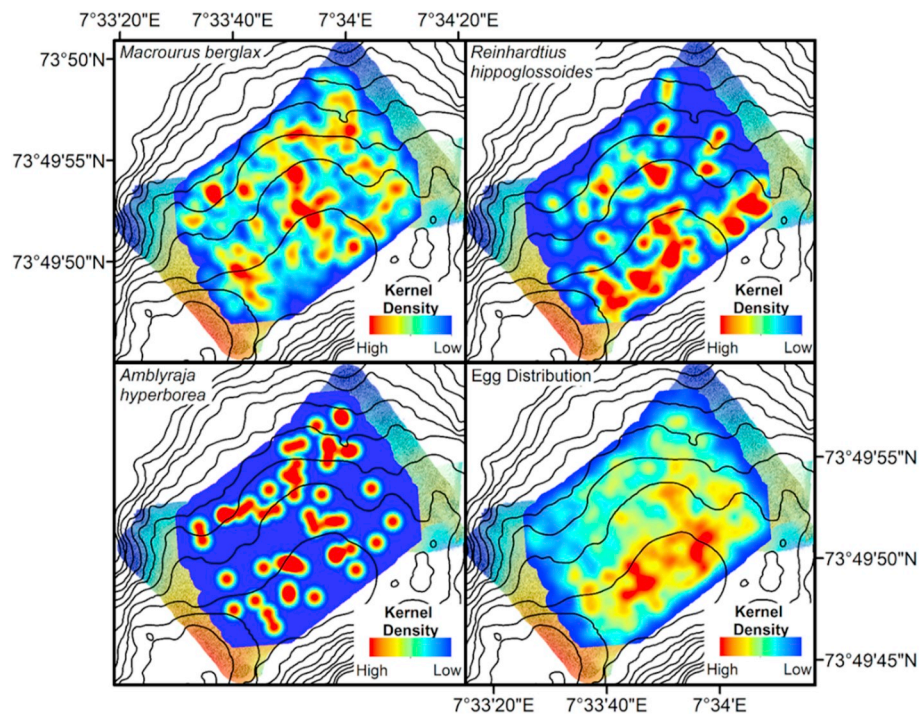
Fig. 6. Kernel density estimation plots of the demersal fish and *Amblyraja hyperborea* egg cases on the Schulz Bank summit determined from the *Hugin 1000* imagery. Contour lines represent every 2 m and are as shown in Fig. 1. Kernel density values are normalized by the maximum densities occurring for each species.

area is situated within a sponge ground. The full spatial extent of the habitat is unknown at this point. However it is likely to extend to a depth of at least 700 m, based on previous results from the Schulz Bank (Roberts et al., 2018).

4.2. Environmental conditions

The measured abiotic variables (temperature, salinity, slope, aspect, and rugosity), with the exception of depth, appeared to have little influence on the patterns displayed by the prominent megafauna. This is unsurprising given the low environmental variability that was observed on the seamount summit during the survey. Temperature and salinity are known to be important variables in the distribution of deep-sea sponge grounds over broad spatial scales (Beazley et al., 2015, 2018; Howell et al., 2016). But over smaller scales, studies have reported depth as the most important variable for demersal communities when compared to other parameters like temperature (Johannesen et al., 2017; Serrano et al., 2017). However, because depth can act as a proxy for many other abiotic variables (Howell et al., 2016), it is possible that unmeasured variables (e.g. local hydrodynamics, suspended matter, and substrate type) that are more sensitive to small-scale variability than the collected parameters are responsible for the patterns observed in the present study.

Roberts et al. (2018) found that the sponge ground on the summit of the Schulz Bank coincided with the boundary between two water masses, Upper Norwegian Deep Water and Norwegian Arctic Intermediate Water. The boundary was particularly dynamic owing to internal waves with a diurnal tidal periodicity and it was concluded that this may benefit the sponges through regular flushing with warmer, oxygen-enriched water from above, the supply of inorganic nutrients and DIC from below by turbulent mixing, and the provision of mechanisms for food supply and the prevention of smothering by sedimentation. The distribution of such 'benefits' over the seamount summit may be uneven as the broader scale seamount hydrodynamics interact with local scale topographic features (e.g. ridges and steep slopes) and this could influence the spatial patterns observed in individual taxa

abiotically in ways not resolved by the present study.

Irrespective of this, given that variability is reduced at small scales (i. e. spatial autocorrelation), it can be hypothesised that community patterns are less likely to be influenced solely by the environment at such scales (Milligan et al., 2016). In such cases, ecological influences like biotic interactions, competition, food and substrate availability, reproduction strategies, and niche partitioning are thought to be major factors driving trends in small-scale community patterns (Mayer and Piepenburg, 1996; Kutti et al., 2013; Sell and Kröncke, 2013; Beazley et al., 2015; Johannesen et al., 2017). Yet, without a more comprehensive study on the influence of the localised environmental and ecological conditions on the individual species spatial patterns, it remains unclear.

4.3. Fine-scale patterns in the megafauna

The *Hugin 1000* AUV proved useful for capturing spatial patterns of the more prominent megafauna such as the ascidians, anemones, hexactinellids, larger demosponges, and fish. The majority of the megafauna were evenly distributed within the small survey area, with the exception of the ascidians, anemones, *L. complicata,* and *G. rubiformis*.

Ascidians and anemones are common inhabitants of sponge grounds (Klitgaard and Tendal, 2004; Hogg et al., 2010; Henry and Roberts, 2014). While the ascidians were often settled directly on the sediments, the anemones were frequently observed growing on the ascidians, large demosponges, and any other available substrate.

The most noteworthy pattern was observed for *L. complicata*, where its density rapidly diminished at depths greater than 586 m. *Lissodendoryx (Lissodendoryx) complicata* is common in arctic slope sponge communities (Mayer and Piepenburg, 1996; Murillo et al., 2018), and has been observed at depths exceeding 1470 m in the Davis Strait (Tompkins et al., 2017), and on the flanks of the Schulz Bank down to 3000 m (Rapp pers. obs.). The clear boundary within the sample area is most likely attributed to random patchiness or biological factors that have yet to be explored.

The lack of distinct spatial patterns produced by the major structure-forming sponges like *G. parva* and *S. rhaphidiophora* is to be expected.

They have a very wide depth range and have been found at depths up to 1997 m on the Schulz Bank in previous surveys (Cárdenas et al., 2013; Roberts et al., 2018). The large demosponges are common hosts to other sponge epibionts, like *H. dedritifera* (Cárdenas et al., 2013). It is likely that some of the other sessile megafaunal spatial patterns are influenced by the large demosponges, as the abundance of structure-forming sponges of the same genera was found to be an important variable in epibenthic megafaunal distribution at the Sackville Spur by Beazley et al. (2015). As an encrusting sponge, *H. dedritifera* is thought to carefully select its host, and therefore its distribution is likely influenced by the host species, substrate type, or the minimum nearest neighbour distance (Cárdenas et al., 2013; Beazley et al., 2015; McIntyre et al., 2016; Hawkes et al., 2019).

Gersemia rubiformis generally occurred in low densities and became more common at the north-western edges of the sample area, though it is common in the arctic benthic ecosystems (Sswat et al., 2015) and has been previously observed in regions dominated by *Geodia* spp. (Jørgensen et al., 2016; Murillo et al., 2016a). Similar to the other prominent megafauna within the sample area, *G. rubiformis* has a wide depth range and it has been documented from 1 m to 3600 m within the northern polar regions (Henry et al., 2003; Murillo et al., 2011, 2016a; Jørgensen et al., 2016). Patchy distribution patterns displayed by *G. rubiformis* in the Atlantic are rather common (Henry et al., 2003) and are thought to be a result of the juvenile settling process where juveniles aggregate at the base of parent colonies on substrate that has already been found to be hospitable by the adults. However, as the species was observed in low quantities, it remains unclear if similar mechanisms or random patchiness are driving the spatial distribution of *G. rubiformis* on the Schulz Bank.

4.4. Demersal fish in sponge grounds

Aggregations of demersal fish are commonly documented on seamounts (Clark et al., 2010) and around sponge grounds (Klitgaard and Tendal, 2004; Kenchington et al., 2013). In the present study, *Macrourus berglax, Reinhardtius hippoglossoides*, and *Amblyraja hyperborea* were consistently observed throughout the sample area and have been reported in other areas dominated by geodiids (Klitgaard and Tendal, 2004; Kenchington et al., 2013; Murillo et al., 2016b). Similar to the findings of Håpnes (2015), these fish species did not display spatial preference for any one particular area of the sponge ground and all fish species were widely and evenly distributed within the sample area.

Since very little is known about *A. hyperborea*, the results from the present survey give some insight on its biogeography and life-history. This skate species is a cold-water species found worldwide and has been observed in sloped regions of the Arctic from depths of 300–1500 m (Skjæraasen and Bergstad, 2001; Doglov et al., 2005; Lynghammar et al., 2013), though it has been reported in low abundances as deep as 1800 m (Stein et al., 2005). Videos collected from ROV surveys conducted on the Schulz Bank showed that *A. hyperborea* and its egg cases are present in lower densities on the flanks of the seamount (unpublished data). *Amblyraja hyperborea* egg cases were consistently observed in high numbers throughout the sample area, though it is uncertain how many egg cases were viable or in the process of degradation at the time of the survey. The presence of skate eggs and juveniles suggests that the area may act as a nursery for *A. hyperborea*, but further research is required to determine habitat specificity.

There is limited understanding of how demersal fish may use sponge grounds. Johannesen et al. (2017) suggest that while sponge grounds do not form feeding links for the fish present, they are likely to be important habitats for fish. Sponge-dominated seamounts have been described as essential habitats for fish species (Sánchez et al., 2008; Sell and Kröncke, 2013; García-Alegre et al., 2014), and evidence suggests that commercial fish catches can be influenced by the presence of such habitats (Rodríguez-Cabello et al., 2009). *Reinhardtius hippoglossoides* is a valued groundfish species that has been commonly associated with sponge

grounds in the past (Kenchington et al., 2013; Beazley et al., 2015; Murillo et al., 2016b), and *A. hyperborea* is a common bycatch within the Greenland Halibut fishery (Peklova et al., 2014).

4.5. Limitations

Similar to findings from Håpnes (2015), the photomosaic facilitated the detection of several megafaunal morphotypes and demersal fish species. However, due to the surveying altitude, image resolution, or the size of the sample area (Sánchez et al., 2008, 2009; Williams et al., 2015), it is likely that the megafaunal densities and species richness were underestimated. Identifying benthic fauna solely with images becomes difficult as the camera lens moves further away from the substrate (Singh et al., 2004), which is consistent with the imagery collected here. Image surveys tend to have poor taxonomic resolution, where many individuals are either too small or cryptic to identify from images alone. This was the case for *G. parva* and *S. rhaphidiophora* as they were often hidden within the spicule mat. A combination of visual and corroborative extractive techniques would allow for a more reliable description of deep-sea habitats and is recommended wherever possible (Howell et al., 2014).

The impact of *Hugin 1000* on the behaviour of the mobile fish species is unknown. Like most visual-based surveying techniques, AUVs are suspected to generate behavioural responses during their surveys and may cause biases from noise or strobe lighting (Raymond and Widder, 2007). This can subsequently impact density estimates of mobile fauna (Stoner et al., 2008; Sánchez et al., 2009; Milligan et al., 2016). However, determining the extent of the impact and type of behavioural response is difficult since it can occur outside of the field of view, and avoidance behaviour may not be accurately captured by still imagery. Therefore, it is critical to heed caution when estimating fish population through imagery data. It is interesting to note that there were numerous incidences of *A. hyperborea* being seemingly unperturbed by the passage of the AUV.

4.6. Conclusion

This study provides insight into community patterns that are often overlooked when surveying deep-sea habitats. Not only were the fine-scale spatial patterns of important arctic sponge ground taxa like *Geodia parva, Stelletta rhaphidiophora, Lissodendoryx (Lissodendoryx) complicata*, and hexactinellid sponges visible, the images also showed demersal fish present in the entire sample area and *Amblyraja hyperborea* potentially using it as a nursery ground. Visual-based surveys are a non-extractive and non-destructive method that allow for the visualisation and characterisation of benthic habitats and give insight into drivers that occur over small-scales (<10's m). Such surveys improve the overall understanding of key species, their fine-scale spatial distribution, and structural habitat of importance to demersal fish (i.e. for nursery grounds), and are thus highly valuable to fisheries, management, and conservation efforts.

Data availability statement

The datasets presented in this article are available at https://doi.org/10.1594/PANGAEA.906904.

Declaration of competing interest

None to declare.

document reflects only the authors' view and the Executive Agency for Small and Medium-sized Enterprises (EASME) is not responsible for any use that may be made of the information it contains. The University of Bergen, Bangor University, and the crew of *RV G.O. Sars* are acknowledged for their contribution to the project for collecting and providing the AUV imagery data for processing. Gokul Raj Krishna is recognised for assisting in the initial processing of the fish survey.

Appendix A. Supplementary data

Supplementary data to this article can be found online at https://doi.org/10.1016/j.dsr.2019.103137.

References

Beazley, L.I., Kenchington, E.L., Murillo, F.J., del Mar Sacau, M., 2013. Deep-sea sponge grounds enhance diversity and abundance of epibenthic megafauna in the Northwest Atlantic. ICES J. Mar. Sci. 70 (7), 1471–1490. https://doi.org/10.1093/icesjms/fst124.

Beazley, L., Kenchington, E., Yashayaev, I., Murillo, F.J., 2015. Drivers of epibenthic megafaunal composition in the sponge grounds of the Sackville Spur, northwest Atlantic. Deep-Sea Res. Part I Oceanogr. Res. Pap. 98, 102–114. https://doi.org/10.1016/j.dsr.2014.11.016.

Beazley, L.I., Wang, Z., Kenchington, E.L., Yashayaev, I., Rapp, H.T., Xavier, J.R., Murillo, F.J., Fenton, D., Fuller, S.D., 2018. Predicted distribution and climatic tolerance of the glass sponge *Vazella pourtalesi* on the Scotian Shelf and its persistence in the face of climatic variability. PLoS One 13 (10), e0205505. https://doi.org/10.1371/journal.pone.0205505.

Bell, J.J., 2008. The functional roles of marine sponges. Estuar. Coast Shelf Sci. 79, 341–353. https://doi.org/10.1016/j.ecss.2008.05.002.

Bell, J.B., Alt, C.H.S., Jones, D.O.B., 2016. Benthic megafauna on steep slopes at the northern mid-atlantic ridge. Mar. Ecol. 37, 1290–1302. https://doi.org/10.1111/maec.12319.

Bett, B.J., Rice, A.L., 1992. The influence of hexactinellid sponge (*Pheronema carpenteri*) spicules on the patchy distribution of macrobenthos in the Porcupine Seabight (bathyal NE Atlantic). Ophelia 36, 217–226. https://doi.org/10.1080/00785326.1992.10430372.

Buhl-Mortensen, L., Vanreusel, A., Gooday, A.J., Levin, L.A., Priede, I.G., Buhl-Mortensen, P., Gheerardyn, H., King, N.J., Raes, M., 2010. Biological structures as a source of habitat heterogeneity and biodiversity on the deep ocean margins. Mar. Ecol. 31, 21–50. https://doi.org/10.1111/j.1439-0485.2010.00359.x.

Cárdenas, P., Xavier, J.R., Reveillaud, J., Schander, C., Rapp, H.T., 2011. Molecular phylogeny of the Astrophorida (Porifera, *Demospongiae*ᴾ) reveals an unexpected high level of spicule homoplasy. PLoS One 6 (4), e18318. https://doi.org/10.1371/journal.pone.0018318.

Cárdenas, P., Rapp, H.T., Klitgaard, A.B., Best, M., Thollesson, M., Tendal, O.S., 2013. Taxonomy, biogeography and DNA barcodes of Geodia species (Porifera, Demospongiae, Tetractinellida) in the Atlantic boreo-arctic region. Zool. J. Linn. Soc-Lond. 169, 251–331. https://doi.org/10.1111/zoj.12056.

Cathalot, C., Van Oevelen, D., Cox, T.J.S., Kutti, T., Lavaleye, M., Duineveld, G., Meysman, F.J.R., 2015. Cold-water coral reefs and adjacent sponge grounds: hotspots of benthic respiration and organic carbon cycling in the deep sea. Front. Mar. Sci. 2 (37), 1–12. https://doi.org/10.3389/fmars.2015.00037.

Clark, M.R., Rowden, A.A., Schlacher, T., Williams, A., Consalvey, M., Stocks, K.I., Rogers, A.D., O'Hara, T.D., White, M., Shank, T.M., Hall-Spencer, J.M., 2010. The ecology of seamounts: structure, function, and human impacts. Annu. Rev. Mar. Sci. 2, 253–278. https://doi.org/10.1146/annurev-marine-120308-081109.

Costello, M.J., McCrea, M., Freiwald, A., Lundälv, T., Jonsson, L., Bett, B.J., Van Weering, T.C.E., De Haas, H., Roberts, J.M., Allen, D., 2005. Role of cold-water *Lophelia pertusa* coral reefs as fish habitat in the NE Atlantic. In: Freiwald, A., Roberts, J.M. (Eds.), Cold-water Corals and Ecosystems. Springer-Verlag, Berlin Heidelberg, pp. 771–805.

Danovaro, R., Snelgrove, P.V., Tyler, P., 2014. Challenging the paradigms of deep-sea ecology. Trends Ecol. Evol. 29, 465–475. https://doi.org/10.1016/j.tree.2014.06.002.

de Goeij, J.M., van Duyl, F.C., 2007. Coral cavities are sinks of dissolved organic carbon (DOC). Limnol. Oceanogr. 52 (6), 2608–2717. https://doi.org/10.4319/lo.2007.52.6.2608.

de Goeij, J.M., van Oevelen, D., Vermeij, M.J.A., Osinga, R., Middelburg, J.J., de Goeij, A.F.P.M., Admiraal, W., 2013. Surviving in a marine desert: the sponge loop retains resources within coral reefs. Science 342 (6154), 108–110. https://doi.org/10.1126/science.1241981.

Doglov, A.V., Grekov, A.A., Shestopal, I.P., Sokolov, K.M., 2005. By-catch of skates in trawl and long-line fisheries in the Barents Sea. J. Northwest Atl. Fish. Sci. 35, 357–366. https://doi.org/10.2960/J.v35.m524.

FAO, 2009. International Guidelines for the Management of Deep-Sea Fisheries in the High Seas. Rome.

Fox, J., Weisberg, S., 2011. An {R} Companion to Applied Regression, second ed. Sage, Thousand Oaks, California. Retrieved from. http://socserv.socsci.mcmaster.ca/jfox/Books/Companion.

García-Alegre, A., Sánchez, F., Gómez-Ballesteros, M., Hinz, H., Serrano, A., Parra, S., 2014. Modelling and mapping the local distribution of representative species on the le danois bank, el cachucho marine protected area (cantabrian sea). Deep-Sea Res. Part I Oceanogr. Res. Pap. 106, 151–164. https://doi.org/10.1016/j.dsr2.2013.12.012.

Grasmueck, M., Eberli, G.P., Viggiano, D.A., Correa, T., Rathwell, G., Luo, J., 2006. Autonomous underwater vehicle (AUV) mapping reveals coral mound distribution, morphology, and oceanography in deep water of the Straits of Florida. Geophys. Res. Lett. 33, L23616. https://doi.org/10.1029/2006GL027734.

Hansen, B., Østerhus, S., 2000. North Atlantic-nordic seas exchanges. Prog. Oceanogr. 45 (2), 109–208. https://doi.org/10.1016/S0079-6611(99)00052-X.

Harrell Jr., F.E., 2018. Package hmisc. Retrieved from. https://cran.r-project.org/web/packages/Hmisc/index.html.

Hawkes, N., Korabik, M., Beazley, L., Rapp, H.T., Xavier, J.R., Kenchington, E.L., 2019. Glass sponge grounds on the Scotian Shelf and their associated biodiversity. Mar. Ecol. Prog. Ser. https://doi.org/10.3354/meps12903.

Henry, L.A., Roberts, J.M., 2014. Applying the OSPAR Habitat Definition of Deep-Sea Sponge Aggregations to Verify Suspected Records of the Habitat in UK Waters. JNCC Report. No. 508.

Henry, L.A., Kenchington, E.L.R., Silvaggio, A., 2003. Effects of mechanical experimental disturbance on aspects of colony responses, reproduction, and regeneration in the cold-water octocoral *Gersemia rubiformis*. Can. J. Zool. 81 (10), 1691–1701. https://doi.org/10.1139/z03-161.

Hogg, M.M., Tendal, O.S., Conway, K.W., Pomponi, S.A., van Soest, R.W.M., Gutt, J., Krautter, M., Roberts, J.M., 2010. Deep-sea Sponge Grounds: Reservoirs of Biodiversity. UNEP-WCMC Biodiversity Series. No. 32. Cambridge.

Hopkins, T.S., 1991. The GIN Sea – a synthesis of its physical oceanography and literature 1972-1985. Earth Sci. Rev. 30, 175–318. https://doi.org/10.1016/0012-8252(91)90001-V.

Howell, K.L., Bullimore, R.D., Foster, N.L., 2014. Quality assurance in the identification of deep-sea taxa from video and image analysis: response to Henry and Roberts. ICES J. Mar. Sci. 71 (4), 899–906. https://doi.org/10.1093/icesjms/fsu052.

Howell, K.L., Piechaud, N., Downie, A.L., Kenny, A., 2016. The distribution of deep-sea sponge aggregations in the North Atlantic and implications for their effective spatial management. Deep-Sea Res. Part I Oceanogr. Res. Pap. 115, 309–320. https://doi.org/10.1016/j.dsr.2016.07.005.

Huvenne, V.A.I., Bett, B.J., Masson, D.G., Le Bas, T.P., Wheeler, A.J., 2016. Effectiveness of a deep-sea cold-water coral Marine Protected Area, following eight years of fisheries closure. Biol. Conserv. 200, 60–69. https://doi.org/10.1016/j.biocon.2016.05.030.

Håpnes, S.J.H., 2015. Mapping of Demersal Fish and Benthos by Autonomous Underwater Vehicle Equipped with Optical and Acoustic Imagers at 600 Meters Depth in Trondheimsfjorden. MSc thesis. Norwegian University of Science and Technology, Trondheim, Norway.

ICES, 2009. Report of the ICES-NAFO Joint Working Group on Deep-Water Ecology (WGDEC), 9–13 March 2009, vol. 23, p. 94. ICES CM 2009\ACOM.

Jeansson, E., Olsen, A., Jutterström, S., 2017. Arctic intermediate water in the nordic seas, 1991–2009. Deep-sea res. Part I: oceanogr. Res. Pap. SO 128, 82–97. https://doi.org/10.1016/j.dsr.2017.08.013.

Jenness, J., 2013. DEM Surface Tools. Jenness Enterprises, Flagstaff.

Johannesen, E., Jørgensen, L.L., Fossheim, M., Primicerio, R., Greenacre, M., Ljubin, P.A., Dolgov, A.V., Ingvaldsen, R.B., Anisimova, N.A., Munhshin, I.E., 2017. Large-scale patterns in community structure of benthos and fish in the Barent Sea. Polar Biol. 40, 237–246. https://doi.org/10.1007/s00300-016-1946-6.

Jørgensen, L.L., Planque, B., Thangstad, T.H., Certain, G., 2016. Vulnerability of megabenthic species to trawling in the Barents Sea. ICES J. Mar. Sci. 73, i84–i97. https://doi.org/10.1093/icesjms/fsv107.

Kelly, D.S., Delaney, J.R., Juniper, S.K., 2014. Establishing a new era of submarine volcanic observatories: cabling axial seamount and the endeavour segment of the Juan de Fuca Ridge. Mar. Geol. 352, 426–450. https://doi.org/10.1016/j.margeo.2014.03.010.

Kenchington, E., Power, D., Koen-Alonso, M., 2013. Association of demersal fish with sponge grounds on the continental slopes of the northwest Atlantic. Mar. Ecol. Prog. Ser. 477, 217–230. https://doi.org/10.3354/meps10127.

Kenchington, E., Murillo, F.J., Lirette, C., Sacau, M., Koen-Alonso, M., Kenny, A., Ollerhead, N., Wareham, V., Beazley, L., 2014. Kernel density surface modelling as a means to identify significant concentrations of vulnerable marine ecosystem indicators. PLoS One 9 (10), e109365. https://doi.org/10.1371/journal.pone.0109365.

Klitgaard, A.B., Tendal, O.S., Westerberg, H., 1997. Mass occurrences of large sponges (Porifera) in Faroe Island (NE Atlantic) Shelf and slope areas: characteristics, distribution and possible causes. In: The Responses of Marine Organisms to Their Environments. Southampton Ocenography Centre, University of Southampton, England, pp. 129–142.

Klitgaard, A.B., Tendal, O.S., 2004. Distribution and species composition of mass occurrences of large-sized sponges in the northeast Atlantic. Prog. Oceanogr. 61, 57–98. https://doi.org/10.1016/j.pocean.2004.06.002.

Knudby, A., Kenchington, E., Murillo, F.J., 2013. Modeling the distribution of *Geodia* sponges and sponge grounds in the Northwest Atlantic. PLoS One 8 (12), e82306. https://doi.org/10.1371/journal.pone.0082306.

Kutti, T., Bannister, R.J., Fosså, J.H., 2013. Community structure and ecological function of deep-water sponge grounds in the Traenadypet MPA – northern Norwegian continental shelf. Cont. Shelf Res. 69, 21–30. https://doi.org/10.1016/j.csr.2013.09.011.

Ludvigsen, M., Sortland, B., Johnsen, G., Singh, H., 2007. Applications of geo-referenced underwater photo mosaics in marine biology and archaeology. Oceanography 20 (4), 140–149. https://doi.org/10.5670/oceanog.2007.14.

Lynghammar, A., Christiansen, J.S., Mecklenburg, C.W., Karamushko, O.V., Møller, P.R., Gallucci, V.F., 2013. Species richness and distribution of chondrichthyan fishes in the Arctic Ocean and adjacent seas. Biodiversity 14 (1), 57–66. https://doi.org/10.1080/14888386.2012.706198.

Maldonado, M., Aguilar, R., Bannister, R.J., Bell, J.J., Conway, K.W., Dayton, P.K., Díaz, C., Gutt, J., Kelly, M., Kenchington, E.L.R., Leys, S.P., Pomponi, S.A., Rapp, H.T., Rützler, K., Tendal, O.S., Vacelet, J., Young, C.M., 2016. Sponge grounds as key marine habitats: a synthetic review of types, structure, functional roles, and conservation concerns. In: Rossi, S., Bramanti, L., Gori, A., Orejas, C. (Eds.), Marine Animal Forests: the Ecology of Benthic Biodiversity Hotspots. Springer, Switzerland, pp. 1–39.

Marsh, L., Copley, J.T., Huvenne, V.A.I., Tyler, P.A., 2013. Getting the bigger picture: using precision remotely operated vehicle (ROV) videography to acquire high-definition mosaic images of newly discovered hydrothermal vents in the Southern Ocean. Deep-Sea Res. Part I Oceanogr. Res. Pap. 92, 124–135. https://doi.org/10.1016/j.dsr2.2013.02.007.

Mauritzen, C., 1996. Production of dense overflow waters feeding the North Atlantic across the Greenland-Scotland Ridge. Part 1: evidence for a revised circulation scheme. Deep-Sea Res. Part I Oceanogr. Res. Pap. 43 (6), 769–806. https://doi.org/10.1016/09670637(96)00037-4.

Mayer, M., Piepenburg, D., 1996. Epibenthic community patterns on the continental slope off East Greenland at 75°N. Mar. Ecol. Prog. Ser. 143, 151–164.

McIntyre, F.D., Neat, F., Collie, N., Stewart, M., Fernandes, P.G., 2015. Visual surveys can reveal rather different 'pictures' of fish densities: comparison of trawl and video camera surveys in the Rockall Bank, NE Atlantic Ocean. Deep-Sea Res. Part I Oceanogr. Res. Pap. 95, 67–74. https://doi.org/10.1016/j.dsr.2014.09.005.

McIntyre, F.D., Drewery, J., Eerkes-Medrano, D., Neat, F.C., 2016. Distribution and diversity of Deep-sea sponge grounds on the rosemary bank seamount, NE atlantic. Mar. Biol. 163 (143) https://doi.org/10.1007/s00227-016-2913-z.

Milligan, R.J., Morris, K.J., Bett, B.J., Durden, J.M., Jones, D.O.B., Robert, K., Ruhl, H.A., Bailey, D.M., 2016. High resolution study of the spatial distributions of abyssal fishes by autonomous underwater vehicle. Sci. Rep. 6, 26095. https://doi.org/10.1038/srep26095.

Morris, K.J., Bett, B.J., Durden, J.M., Huvenne, V.A., Milligan, R., Jones, D.O.B., McPhail, S., Robert, K., Bailey, D.M., Ruhl, H.A., 2014. A new method for ecological surveying of the abyss using autonomous underwater vehicle photography. Limnol Oceanogr. Methods 12, 795–809. https://doi.org/10.4319/lom.2014.12.795.

Murillo, F.J., Durán Muñoz, P., Altuna, A., Serrano, A., 2011. Distribution of deep-water corals of the flemish Cap, flemish pass, and the grand banks of newfoundland (Northwest Atlantic ocean): interaction with fishing activities. ICES J. Mar. Sci. 68 (2), 319–332. https://doi.org/10.1093/icesjms/fsq071.

Murillo, F.J., Durán Muñoz, P., Cristobo, J., Ríos, P., González, C., Kenchington, E., Serrano, A., 2012. deep-sea sponge grounds of the flemish Cap, flemish pass and the grand banks of newfoundland (Northwest Atlantic ocean): distribution and species composition. Mar. Biol. 8 (9), 842–854. https://doi.org/10.1080/17451000.2012.682583.

Murillo, F.J., Serrano, A., Kenchington, E., Mora, J., 2016. Epibenthic assemblages of the Tail of the Grand Bank and Flemish Cap (northwest Atlantic) in relation to environmental parameters and trawling intensity. Deep-Sea Res. Part I Oceanogr. Res. Pap. 109, 99–122. https://doi.org/10.1016/j.dsr.2015.08.006.

Murillo, F.J., Kenchington, E., Lawson, J.M., Li, G., Piper, D.J.W., 2016. Ancient Deep-sea sponge grounds on the flemish Cap and grand bank, Northwest Atlantic. Mar. Biol. 163, 63. https://dx.doi.org/10.1007%2Fs00227-016-2839-5.

Murillo, F.J., Kenchington, E., Tompkins, G., Beazley, L., Baker, E., Knudby, A., Walkusz, W., 2018. Sponge assemblages and predicted archetypes in the eastern Canadian Arctic. Mar. Ecol. Prog. Ser. 597, 115–135. https://doi.org/10.3354/meps12589.

Olsen, B.R., Troedsson, C., Hadziavdic, K., Pederson, R.B., Rapp, H.T., 2015. The influence of vent systems on pelagic eukaryotic micro-organism composition in the Nordic Seas. Polar Biol. 38, 547–558. https://doi.org/10.1007/s00300-014-1621-8.

Orvik, K.A., Niiler, P., 2002. Major pathways of atlantic water in the northern North Atlantic and nordic seas toward arctic. Geophys. Res. Lett. 29 (19), 1896. https://doi.org/10.1029/2002GL015002.

OSPAR, 2008. OSPAR List of Threatened And/or Declining Species and Habitats (Reference Number: 2008-6). London.

Pedersen, R.B., Rapp, H.T., Thorseth, I.H., Lilley, M.D., Barriga, F.J.A.S., Baumberger, T., Flesland, K., Fonseca, R., Früh-Green, G.L., Jorgensen, S.L., 2010. Discovery of a black smoker vent field and vent fauna at the Arctic Mid-Ocean Ridge. Nat. Commun. 1, 123. https://doi.org/10.1038/ncomms1124.

Peklova, I., Hussey, N.E., Hedges, K.J., Treble, M.A., Fisk, A.T., 2014. Movement, depth and temperature preferences of an important bycatch species, Arctic skate *Amblyraja hyperborea*. In: Cumberland Sound, Canadian Arctic. Endanger. Species Res, vol.23, pp. 229–240. https://doi.org/10.3354/esr00563.

Plotkin, A., Gerasimova, E., Rapp, H.T., 2018. Polymastiidae (Porifera: Demospongiae) of the nordic and siberian seas. J. Mar. Biol. Assoc. U. K. 98 (6), 1273–1335. https://doi.org/10.1017/S0025315417000285.

Powell, A., Clarke, M.E., Fruh, E., Chaytor, J.D., Reiswig, H.M., Whitmire, C.E., 2018. Characterizing the sponge grounds of grays canyon, Washington, USA. Deep-Sea Res. Part II Top. Stud. Oceanogr. 150, 146–155. https://doi.org/10.1016/j.dsr2.2018.01.004.

Raymond, E.H., Widder, E.A., 2007. Behavioral responses of two deep-sea fish species to red, far-red, and white light. Mar. Ecol. Prog. Ser. 350, 291–298. https://doi.org/10.3354/meps07196.

Rodríguez-Cabello, C., Sánchez, F., Ortiz de Zarate, V., Barreiro, S., 2009. Does le danois bank (el cachucho) influence albacore catches in the cantabrian sea? Cont. Shelf Res. 29 (8), 1205–1212. https://doi.org/10.1016/j.csr.2008.12.018.

Robert, K., Jones, D.O.B., Huvenne, V.A., 2014. Megafaunal distribution and biodiversity in a heterogeneous landscape: the iceberg-scoured Rockall Bank, NE Atlantic. Mar. Ecol. Prog. Ser. 501, 67–88. https://doi.org/10.3354/meps10677.

Robert, K., Huvenne, V.A.I., Georgiopoulou, A., Jones, D.O.B., Marsh, L., Cater, G.D.O., Chaumillon, L., 2017. New approaches to high-resolution mapping of marine vertical structures. Sci. Rep. 7, 9005. https://doi.org/10.1038/s41598-017-09382-z.

Roberts, E.M., Mienis, F., Rapp, H.T., Hanz, U., Meyer, H.K., Davies, A.J., 2018. Oceanographic setting and short-timescale environmental variability at an Arctic seamount sponge ground. Deep-Sea Res. Part I Oceanogr. Res. Pap. 138, 98–113. https://doi.org/10.1016/j.dsr.2018.06.007.

RStudio Team, 2016. RStudio. Integrated Development for R. RStudio, Inc., Boston, Massachusetts. Retrieved from. http://www.rstudio.com/.

Sánchez, F., Serrano, A., Parra, S., Ballesteros, M., Cartes, J.E., 2008. Habitat characteristics as determinant of the structure and spatial distribution of epibenthic and demersal communities of Le Danois Bank (Cantabrian Sea, N. Spain). J. Mar. Syst. 72, 64–86. https://doi.org/10.1016/j.jmarsys.2007.04.008.

Sánchez, F., Serrano, A., Ballesteros, M.G., 2009. Photogrammetric quantitative study of habitat and benthic communities of deep Cantabrian Sea hard grounds. Cont. Shelf Res. 29, 1174–1188. https://doi.org/10.1016/j.csr.2009.01.004.

Sell, A.F., Kröncke, I., 2013. Correlations between benthic habitats and demersal fish assemblages – a case study on the Dogger Bank (North Sea). J. Sea Res. 80, 12–24. https://doi.org/10.1016/j.seares.2013.01.007.

Serrano, A., Cartes, J.E., Papiol, V., Punzón, A., Garciá-Alegre, A., Arronte, J.C., Ríos, P., Lourido, A., Frutos, I., Blanco, M., 2017. Epibenthic communities of sedimentary habitats in a NE Atlantic deep-seamount (Galicia Bank). J. Sea Res. 130, 154–165. https://doi.org/10.1016/j.seares.2017.03.004.

Silverman, B.W., 1986. Density Estimation for Statistics and Data Analysis. Chapman and Hall, New York.

Singh, H., Armstrong, R., Gilbes, F., Eustice, R., Roman, C., Pizarro, O., Torres, J., 2004. Imaging coral I: imaging coral habitats with the SeaBED AUV. P. Soc. Photo-Opt. Ins. 5 (1), 25–42. https://doi.org/10.1023/B:SSTA.0000018445.25977.f3.

Skjæraasen, J.E., Bergstad, O.A., 2001. Notes on the distribution and length composition of *Raja lintea, R. fyllae, R. hyperborea*, and *Bathyraja spinicauda* (Pisces: rajidae) in the deep northeastern North Sea and on the slope of the eastern Norwegian Sea. ICES J. Mar. Sci. 58, 21–28. https://doi.org/10.1006/jmsc.2000.0985.

Sswat, M., Gulliksen, B., Menn, I., Sweetman, A.K., Piepenburg, D., 2015. Distribution and composition of the epibenthic megafauna north of Svalbard (Arctic). Polar Biol. 38, 861–877. https://doi.org/10.1007/s00300-015-1645-8.

Statham, P.J., Connelly, D.P., German, C.R., Brand, T., Overnell, J.O., Bulukin, E., Millard, N., McPhail, S., Pebody, M., Perrett, J., Squire, M., Stevenson, P., Webb, A., 2005. Spatially complex distribution of dissolved manganese in a fjord as revealed by high-resolution in situ sensing using the autonomous underwater vehicle Autosub. Environ. Sci. Technol. 39 (24), 9440–9445. https://doi.org/10.1021/es050980t.

Steen, I.H., Dahle, H., Stokke, R., Roalkvam, I., Daae, F.L., Rapp, H.T., Pedersen, R.B., Thorseth, I.H., 2016. Novel barite chimneys at the Loki's Castle Vent Field shed light on key factors shaping microbial communities and functions in hydrothermal systems. Front. Microbiol. 6 https://doi.org/10.3389/fmicb.2015.01510 article 1510.

Stein, D.L., Felley, J.D., Vecchione, M., 2005. ROV observations of benthic fishes in the northwind and Canada basins, arctic ocean. Polar Biol. 28, 232–237. https://doi.org/10.1007/s00300-004-0696-z.

Stoner, A.W., Ryer, C.H., Parker, S.J., Auster, P.J., Wakefield, W.W., 2008. Evaluating the role of fish behaviour in surveys conducted with underwater vehicles. Can. J. Fish. Aquat. Sci. 65, 1230–1243. https://doi.org/10.1139/F08-032.

Thresher, R., Althaus, F., Adkins, J., Gowlett-Holmes, K., Alderslade, P., Dowdney, J., Cho, W., Gagnon, A., Staples, D., McEnnulty, F., Williams, A., 2014. Strong depth-related zonation of megabenthos on a rocky continental margin (~700-4000 m) off Southern Tasmania, Australia. PLoS One 9 (1), e85872. https://doi.org/10.1371/journal.pone.0085872.

Tompkins, G., Baker, E., Antsey, L., Walkusz, W., Siferd, T., Kenchington, E., 2017. Sponges from the 2010-2014 paamiut multispecies trawl surveys, eastern arctic and subarctic: class Demospongiae, subclass heteroscleromorpha, order poecilosclerida, family coelosphaeridae, genera *forcepia* and *Lissodendoryx*. Can. Tech. Rep. Fish. Aquat. Sci. No. 3224.

Williams, A., Althaus, F., Schlacher, T.A., 2015. Towed camera imagery and benthic sled catches provide different views of seamount benthic diversity. Limnol Oceanogr. Methods 13, 62–73. https://doi.org/10.1002/lom3.10007.

Wood, S.N., 2011. Fast stable restricted maximum likelihood and marginal estimation of semiparametric generalized linear models. J. R. Stat. Soc. B. 73 (1), 3–36.

Wynn, R.B., Huvenne, V.A.I., Le Bas, T.P., Murton, B.J., Connelly, D.P., Bett, B.J., Ruhl, H.A., Morris, K.J., Peakall, J., Parsons, D.R., Sumner, E.J., Darby, S.E., Dorrell, R.M., Hunt, J.E., 2014. Autonomous Underwater Vehicles (AUVs): their past, present and future contribution to the advancement of marine geoscience. Mar. Geol. 352, 451–468. https://doi.org/10.1016/j.margeo.2014.03.012.

Zuur, A.F., Ieno, E.N., Walker, N.J., Saveliev, A.A., Smith, G.M., 2009. Mixed Effect Models and Extensions in Ecology with R. Statistics for Biology and Health. Springer Science + Business Media, New York, p. 574.